Electronic Supporting Information

Tracing Mechanistic Pathways and Reaction Kinetics Toward Equilibrium in Reactive Molten Salts

Luke D. Gibson,[a] Santanu Roy,*[b] Rabi Khanal,[a] Rajni Chahal,[b] Ada Sedova,[c] and Vyacheslav S. Bryantsev**[b]

[a]Computational Sciences and Engineering Division, Oak Ridge National Laboratory, P.O. Box 2008, Oak Ridge, TN 37831

[b]Chemical Science Division, Oak Ridge National Laboratory, P.O. Box 2008, Oak Ridge, TN 37831

[c]Bioscience Division, Oak Ridge National Laboratory, P.O. Box 2008, Oak Ridge, TN 37831

Corresponding Authors
*Santanu Roy (roys@ornl.gov)
**Vyacheslav S. Bryantsev (bryantsevv@ornl.gov)

Theory and Computational Methods

1. Collective variables representing coordination environments

1.1 Coordination numbers

Considering r_i as the distance between the i^{th} Cl^- and Al^{3+} and $r^\dagger$ as the location of the boundary of the first chloride coordination shell determined from the first minimum of the Al^{3+}-Cl^- RDF, the Cl^- coordination number of an Al^{3+} ion is given by:

$$CN_{\mathrm{Al}}^{\mathrm{Cl}} = \sum_{i=1}^{N_{\mathrm{Cl}}} \frac{1-\left(\frac{r_i}{r^\dagger}\right)^{12}}{1-\left(\frac{r_i}{r^\dagger}\right)^{24}} = \sum_{i=1}^{N_{\mathrm{Cl}}} f_i^{\mathrm{Cl}} \qquad (S1)$$

Here, f ($0 < f < 1$) is a smooth function that allows smooth transitions of Cl^- across the boundary of the first chloride solvation shell. N_{Cl} is the total number of Cl^- ions. Similarly, the Al^{3+} coordination number of a Cl^- ion is expressed as:

$$CN_{\mathrm{Cl}}^{\mathrm{Al}} = \sum_{i=1}^{N_{\mathrm{Al}}} \frac{1-\left(\frac{r_i}{r^\dagger}\right)^{12}}{1-\left(\frac{r_i}{r^\dagger}\right)^{24}} = \sum_{i=1}^{N_{\mathrm{Al}}} f_i^{\mathrm{Al}} \qquad (S2),$$

where, N_{Al} represents the total number of Al^{3+} ions. Equations 1 and 2 are useful for determining the distribution and metastability of coordination structures from MD trajectories. The powers, 12 and 24, were chosen based on our previous study that showed that these powers are optimal for predicting accurate CN while maintaining its smooth variation.[1] The associated free energy profiles are linked to the CN distributions (P(CN)) through the relation: $W(CN) = -k_B T \ln(P(CN))$, where T is the temperature and k_B is the Boltzmann constant. CN_{Cl}^{K} has the same form as CN_{Cl}^{Al}, while $r^\dagger$ is computed from the K-Cl RDF.

1.2 Number of shared Cl^-/Al^{3+} between two Al^{3+} ions. In Equation 1, f_i^{Cl} is the contribution of the i^{th} Cl^- to the coordination structure of an Al^{3+} ion. Therefore, f_{ij}^{Cl} and f_{ik}^{Cl} can be treated as the contributions of the i^{th} Cl^- respectively to the coordination structures of the j^{th} and k^{th} Al^{3+} ions. Then, the number of Cl^- ions shared between these two Al^{3+} ions is given by:

$$n_{\mathrm{Cl}}^{\mathrm{Shared}} = \sum_{i=1}^{N_{\mathrm{Cl}}} f_{ij}\, f_{ik} \qquad (S3)$$

The number of Al^{3+} ions coordinating with two different Al^{3+} ions (*j* and *k*) through chloride sharing ($n_{\mathrm{Al}}^{\mathrm{Shared}}$) is given by:

$$n_{\mathrm{Al}}^{\mathrm{Shared}} = \sum_{i=1(\neq j,\neq k)}^{N_{\mathrm{Al}}} f_{ij}\, f_{ik} \qquad (S4)$$

Herein, *f* is obtained by using $r^{\dagger}$ from the Al^{3+}-Al^{3+} RDF. The 2D free energy surfaces, $W\left(r_{\text{Al-Al}}, n_{\mathrm{Cl}}^{\mathrm{Shared}}\right)$ and $W(r_{\text{Al-Al}}, n_{\mathrm{Al}}^{\mathrm{Shared}})$, are computed from the joint probability distributions (P) of *r* and *n:* $W\left(r_{\text{Al-Al}}, n_{\mathrm{Cl}}^{\mathrm{Shared}}\right) = -k_B T\, ln[P(r_{\text{Al-Al}}, n_{\mathrm{Cl}}^{\mathrm{Shared}})]$ and $W\left(r_{\text{Al-Al}}, n_{\mathrm{Al}}^{\mathrm{Shared}}\right) = -k_B T\, ln[P(r_{\text{Al-Al}}, n_{\mathrm{Al}}^{\mathrm{Shared}})]$.

2. Survival probability correlation function

The survival probability, $P(t,t+\delta t)$, of a Cl^- ion in the first coordination shell of an Al^{3+} ion is assigned to 1 when the Cl^- is found in the first shell at both times *t* and $t+\delta t$. Otherwise, *P* is assigned to 0. Then the survival probability correlation function is determined as:

$$C(t) = \langle P(t,t+\delta t)\rangle_{i,t} / \langle P(t,t)\rangle_{i,t} \qquad (S5)$$

where $\langle\ldots\rangle_{i,t}$ indicates averaging over all Al-Cl pairs and time. Likewise, $C(t)$ can be calculated for Al-Al pairs. The boundary of the coordination shells is determined from the location of the first minimum of the Al-Cl and Al-Al RDFs.

3. A Marcus-like theory

Recently a rate theory based on Marcus theory[2, 3] has been extended for the electric field reaction coordinate,[4, 5] where the reactant (R) and product (P) states of a reaction are defined as the parabolic functions of *E*:

$$W_{\mathrm{R}}(E) = W_{\mathrm{R}} + \frac{1}{2}K_{\mathrm{R}}(E-E_{\mathrm{R}})^2$$
$$W_{\mathrm{P}}(E) = W_{P} + \frac{1}{2}K_{\mathrm{P}}(E-E_{\mathrm{P}})^2 \qquad (S6),$$

where, W_{R} and W_{P} are the minima of the reactant product parabolas located respectively at $E = E_{\mathrm{R}}$ and $E = E_{\mathrm{P}}$. K_{R} and K_{P} are the curvatures of these parabolas, respectively. *E* is calculated for two cases. First, considering all possible Al-Cl pairs, *E* is determined as the projection of the electric field exerted on a chloride ion by all other ions along the Al-Cl direction ($\hat{r}$). That is, $E = \hat{r}.\sum_{j=1}^{N-1}\frac{Q_i}{{r_i}^2}\hat{r_i}$, where Q_i is the formal charge of the i^{th} ion located at a distance r_i and *N* is the total number of ions. Second, considering all possible Al-Al pairs, *E* is obtained as the projection of the electric field exerted on an Al^{3+} ion along the Al-Al direction using the same expression. Based on all possible Al-Cl or Al-Al pairs for different Al-Cl distances ($r_{\text{Al-Cl}}$) or Al-Al distances ($r_{\text{Al-Al}}$), *E* on Cl or Al was determined, which allowed us to compute the distance-electric field joint probability distribution and the associated 2D free energy surface. Since the reaction rate calculations were only done for the Al-Al dissociation case, $W_{\mathrm{R}}(E)$ and $W_{\mathrm{P}}(E)$ in Equation S6 are determined from the parabolic fits to a couple of slices extracted from these 2D surfaces (W(r, E)) respectively along the equilibrium distances in the reactant close-contact ($r = r_R$) and the product solvent-separated ($r = r_P$) Al-Al states. These parabolas represent the reactant and product diabats that cross at a point ($E^{\dagger}$) treated as the transition state. The lower (W_-) and higher (W_+) adiabatic free energy surfaces are constructed by accounting for the coupling (*C*) between the diabats, i.e., $W_{\pm} = \frac{W_{\mathrm{R}}(E)+W_{\mathrm{P}}(E)}{2} \pm \frac{1}{2}\sqrt{4[C(E)]^2 + [W_{\mathrm{R}}(E) - W_{\mathrm{P}}(E)]^2}$.[4, 5] Here, the coupling constant *C* is expressed $\frac{K_{\mathrm{R}}+K_{\mathrm{P}}}{2\sqrt{K_{\mathrm{R}}K_{\mathrm{P}}}}\sqrt{[W_{\mathrm{R}}(E) - W_{\mathrm{R}}][W_{\mathrm{P}}(E) - W_{\mathrm{P}}]}$, where the prefactor disappears when both the parabolas have equal curvatures ($K_{\mathrm{R}} = K_{\mathrm{P}}$). In an exact Marcus theory, when a trajectory arrives at the crossing point,

it immediately goes to the product equilibrium. However, two key factors may delay the transition. First, an additional barrier may exist along the Al-Al distance at the crossing point. Second, the recrossing events of the crossing point that is accounted for by computing the transmission coefficient. Therefore, the transition rate takes the form of:[4, 5]

$$k_E = \kappa_{\mathrm{LZ}} \sqrt{\frac{Z_E}{2\pi\beta}} \frac{e^{-\beta\left[W(E^\dagger)+\Delta W_r^{E^\dagger}\right]}}{\int_{E_i}^{E^\dagger} dE\, e^{-\beta W(E)}}$$

$$= \kappa_{LZ} \sqrt{\frac{1}{2\pi\beta}} \frac{e^{-\beta W_{\mathrm{Tot}}}}{\frac{1}{\sqrt{Z_E}} V_{\mathrm{R}}^E} \qquad (S7).$$

Here, *W(E)=W_*(E) is the lower adiabatic free energy surface and $W\left(E^\dagger\right)$ is the barrier top on this surface. $\Delta W_r^{E^\dagger}$ is the additional barrier along the Al-Al distance, providing a total barrier of W_{Tot}. $\beta = 1/k_{\mathrm{B}}T$ represents inverse thermal energy and B is the Boltzmann constant. The integral from $\boldsymbol{E_i}$ to $\boldsymbol{E}^\dagger$ provides the "reactant volume" in the electric field space (V_R^E). $1/Z_E$ is the mass associated with the electric field motion, and $\left(1/\sqrt{Z_E}\right)V_R^E$ is the mass-weighted "reactant volume". κ_{LZ} is the transmission coefficient obtained by employing the semiclassical approach of Landau and Zener.[3, 6, 7] The probability (P) of reactive transitions through the crossing region and the location of the crossing region control $\boldsymbol{\kappa_{\mathrm{LZ}}}$ through the relations: $\kappa_{\mathrm{LZ}} = 2P/(P+1)$ for the parabolas crossing at the "normal" region (opposite side) and $\boldsymbol{\kappa_{\mathrm{LZ}}} = 2P(1-P)$ for the parabolas crossing at the "inverted" region (same side). *P* depends on the coupling strength between the parabolas and the mean traversal velocity of the electric field ($\overline{\boldsymbol{v}}_{\boldsymbol{E}}$) at the crossing point, $E^\dagger$: $P = 1 - \exp\left[-\frac{2\pi\left[C(E^\dagger)\right]^2}{\hbar|\bar{v}_E||S_2-S_1|}\right]$, where $\hbar = h/2\pi$ and h is the Planck constant. $S_{1,2} = \frac{dW(E)}{dE}|_{E=E^\dagger}$ represents the slopes of the parabolas at the crossing point. We find that the trajectories traversing the crossing point show a Gaussian velocity distribution expressed as $D(|\mathrm{v}_E|) = \mathrm{D}_0 \exp[-|v_E|^2/\sigma^2]$, and therefore, the mean velocity is obtained from $|\bar{v}_E| = \int |\mathrm{v}_E|\, D(|\mathrm{v}_E|)\, \mathrm{d}|\mathrm{v}_E|$. All parameters used for Marcus theory-based analysis are given in Table S1.

4. PIM simulation

The pure $AlCl_3$ system contains a set of ($30Al^{3+}$, $90Cl^-$) ions, while the systems with 66.7 mol%, 58 mol%, and 50 mol% of $AlCl_3$ contain sets of ($32Al^{3+}$, $16K^+$, $112Cl^-$), ($28Al^{3+}$, $20K^+$, $104Cl^-$), and ($22Al^{3+}$, $22K^+$, $88Cl^-$) ions, respectively. First, we performed the PIM[8] simulation in the NPT (constant number of ions, pressure, and temperature) ensemble for 1 ns at 1 bar and at 498 K (for pure $AlCl_3$ and the mixture with the 66.7 mol% of $AlCl_3$) and at 573 K (the mixtures with the 58 mol% and 50 mol% of $AlCl_3$). Temperature and pressure were controlled using the Nosé-Hoover[9, 10] thermostat and barostat. Then we extracted configurations from these NPT trajectories corresponding to the experimental densities, 1.212 g/cm^3, 1.596 g/cm^3, 1.537 g/cm^3, and 1.576 g/cm^3, respectively for pure $AlCl_3$ and the mixture with the 66.7 mol%, 58 mol%, and 50 mol% of $AlCl_3$. The resulting cubic cell dimensions were 17.630 Å, 17.842 Å, 17.804 Å, 16.890 Å, respectively. We ran another 1 ns PIM simulation in the NVT (constant number of ions, volume, and temperature) ensembles using those extracted configures for each system. All PIM simulations were performed using 1 femtosecond (fs) MD timestep. The electrostatic interactions were treated with EWALD summation method.[11] The cutoff for the non-bonded interaction was set to 8 Å.

5. AIMD simulation

All AIMD simulations were carried out using 1.0 fs timestep by employing the Quickstep module of the CP2K package[12, 13] in the NVT ensembles. We used the PBE[14-16] exchange-correlation functional with Grimme's D3 dispersion correction[17] and the MOLOPT(DZVP)[18] basis set along with the Goedecker-Teter-Hutter[19] (GTH) pseudopotentials for all ions. PBE-D3 has been demonstrated to generate good local coordination structures for multivalent cation salts by accurately reproducing experimental spectra features in simulated Raman spectroscopy.[20] A 600 Ry density cutoff for the plane wave basis was applied. The Nosé-Hoover[9, 10, 21] thermostat with a 1.0 ps time constant was used for the temperature coupling.

6. Raman Spectroscopy: Computed spectra and their alignment with experimental ones

Raman spectra were computed from the AIMD trajectories using a previously developed formalism[20, 22] by performing a Fourier transformation of the time-autocorrelation functions of the polarizability tensor components. The polarizability tensor is computed from induced dipole moments of the full periodic simulation cell using the Berry phase[23, 24] method implemented in CP2K.[12, 25]

The wavenumbers for the simulated 50 and 100 mol% $AlCl_3$ compositions were multiplied by scaling factors of 1.052 and 1.062 to align the main peak position at 341 and 350 cm^{-1} in the experimental spectra, respectively. The wavenumbers for the simulated 58 and 66.7 mol% $AlCl_3$ spectra were also multiplied by a scaling factor of 1.052 for consistency. The zero-intensity reference for each computed spectra was aligned with their corresponding experimental spectra at 650 cm^{-1}. After alignment, the intensities of 50, 66.7, and 100 mol% $AlCl_3$ were multiplied by a scaling factor such that the error (RMSE) between their respective experimental peaks was minimized. For 66.7 mol% $AlCl_3$, only the converged spectrum was used to determine the scaling factor. For 58 mol% $AlCl_3$, however, the experimental spectrum exhibits a nonphysical drop below zero intensity in the 200-300 cm^{-1} region, and we thus scaled the two computed 58 mol% $AlCl_3$ spectra by hand. The same scaling factor was used for both the converged and unconverged spectra in the cases of 58 and 66.7 mol% $AlCl_3$.

Raman spectra calculations on small gas clusters were conducted using the Gaussian 16 RevA.03 code.[26] For geometry optimization and frequency calculations, we utilized the PBE-D3[14-17] density function along with the 6-311+G(d,p) basis.

7. Speciation and Reaction Analysis

Speciation was determined using the AGGREGATES[27] code to detect aggregates with an A-B-A-B pattern, where A and B are Al^{3+} and Cl^- ions, respectively. A cutoff value of 3.03 Å was used to determine Al-Cl connectivity in the aggregate analysis. The average population of each aggregate was computed in 30 ps intervals for 58 and 66.7 mol% $AlCl_3$, which is plotted in **Figures 1** (in main text) and **S1**. Chemical reactions in 58 and 66.7 mol% $AlCl_3$ trajectories were determined by constructing graph[28] representations of Al-Cl aggregates ($r_{\mathrm{cut}}^{(\mathrm{Al-Cl})}$ = 3.03 Å) in each frame and detecting changes in the Al-Cl graph topologies for adjacent frames. We confirmed that this graph-based approach[28] produces the same speciation distributions as AGGREGATES.[27]

Supporting Figures

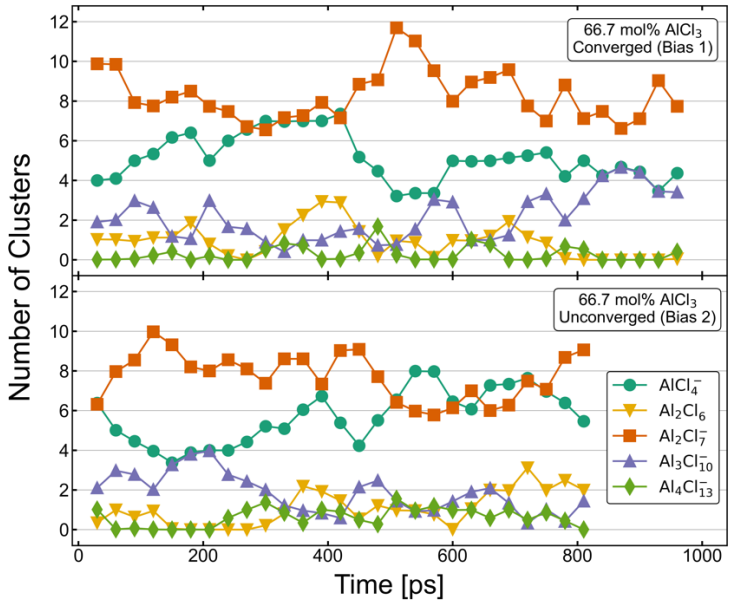

Figure S1. Species distribution over time obtained from aggregate analysis for Bias 1 and Bias 2 trajectories of 66.7 mol% of $AlCl_3$.

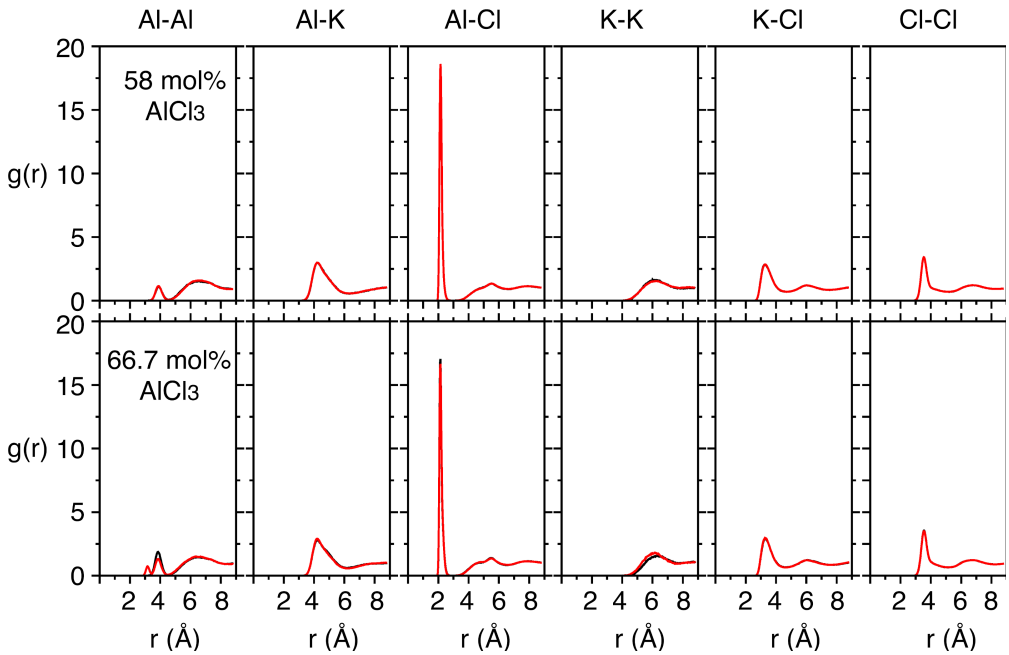

Figure S2. Radial distribution functions showing that they are almost identical in the non-equilibrium (red) and equilibrium (black) parts of the AIMD trajectories.

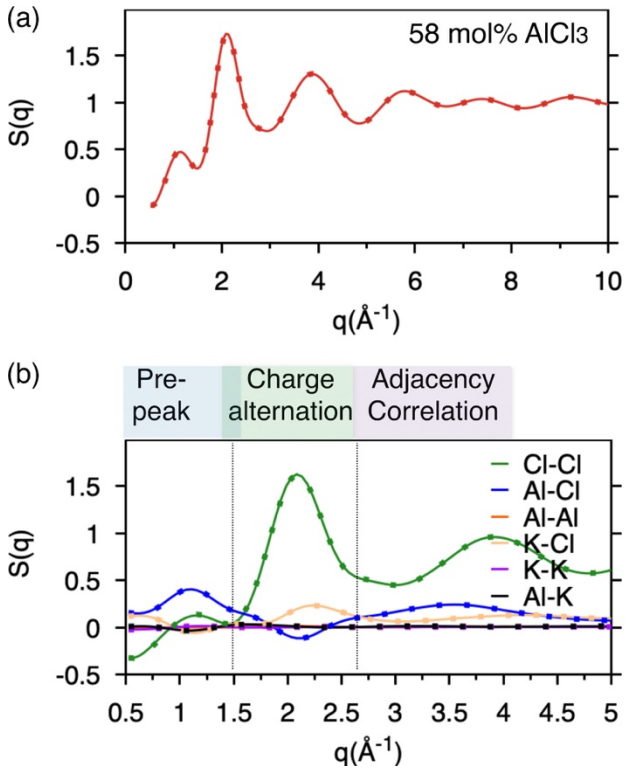

Figure S3. Computed total and partial structure functions for the 58 mol % of $AlCl_3$. Solid lines and dots indicate Bias 1 and Bias 2, respectively.

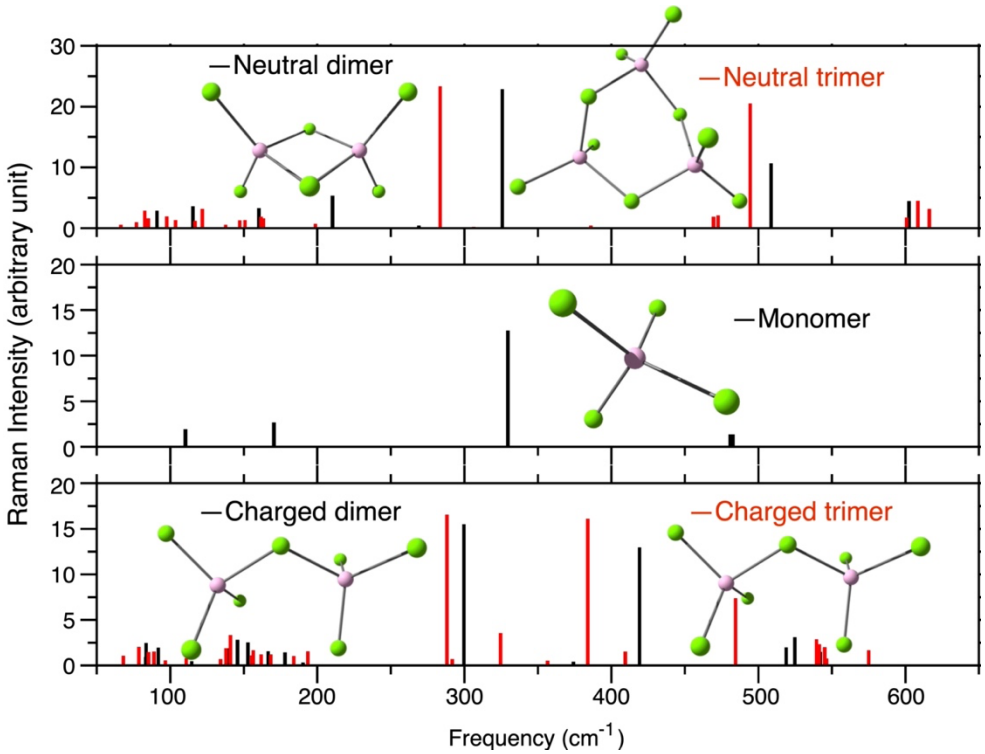

Figure S4. The snapshots of gas-phase optimized species and their Raman spectra: neutral dimer and trimer, (top) charged monomer (middle), and charged dimer and trimer (bottom).

Supporting Tables

Table S1. Parameters of the extended Marcus theory: *(1)* Marcus parabolas presented by the reactant $W_{\mathrm{R}}(E) = W_{\mathrm{R}} + \frac{1}{2}K_{\mathrm{R}}(E - E_{\mathrm{R}})^2$ and the product $W_{\mathrm{P}}(E) = W_P + \frac{1}{2}K_{\mathrm{P}}(E - E_{\mathrm{P}})^2$, where W_{R} and W_{P} are the minima, E_{R} and E_{P} are the locations of the minima, and K_{R} and K_{P} are the curvatures for the reactant and product states, respectively. *(2)* The barrier at the electric field transition state is $W\left(E^{\dagger}\right)$, which is accompanied by an additional barrier along *r* ($\Delta W_r^{E^{\dagger}}$) at this transition state. *(3)* The transmission coefficient κ_{LZ} depends on the probability of reaction transition *P* that is obtained as $P = 1 - \exp\left[-\frac{2\pi\left[C\left(E^{\dagger}\right)\right]^2}{\hbar|\bar{v}_E||S_2 - S_1|}\right]$, where $\hbar = h/2\pi$ (*h* is the Planck constant), $S_{1,2} = \frac{dW(E)}{dE}|_{E=E^{\dagger}}$, and are the slopes of the parabolas at the crossing point. The trajectories traversing the crossing point exhibit a Gaussian velocity distribution in the form of $D(|\mathrm{v}_E|) = \mathrm{D}_0 \exp[-|v_E|^2/\sigma^2]$, and the mean velocity is obtained from $v_E^{\mathrm{Mean}} = \int |\mathrm{v}_E|\ D(|\mathrm{v}_E|)\ \mathrm{d}|\mathrm{v}_E|$. *(4)* The value of the inverse mass Z_E, which is a conserved quantity that fluctuates over time due to the thermal fluctuation of ions, is obtained through averaging over the production run of the AIMD trajectories.

	58 mol% of $AlCl_3$	66.7 mol% of $AlCl_3$
<u>Marcus parabolas</u> W_R W_P (kcal/mol)	 0.3038010 0.0112701	 -0.061328 0.435084
E_R E_P $(\frac{E_h/\mathrm{Bohr}}{e})$	0.0211689 -0.00242981	0.0203871 -0.00283846
K_R K_P [kcal mol^{-1}/ $(\frac{E_h/\mathrm{Bohr}}{e})^2$]	5840.52 4871.81	5105.53 3251.43
<u>Barriers</u> $W\left(E^{\dagger}\right)$ $\Delta W_r^{E^{\dagger}}$ $\left[W\left(E^{\dagger}\right) + \Delta W_r^{E^{\dagger}}\right]$ (kcal/mol)	 0.186925 3.45 3.636925	 0.290071 2.8 3.090071
$e^{-\beta\left[W\left(E^{\dagger}\right)+\Delta W_r^{E^{\dagger}}\right]}$	0.041007	0.044049
<u>Mass and reactant volume</u> Z_E (e^2 nm^{-6}/g mol^{-1}) Reactant volume V_R^E	8876.65	9685.16

$(\frac{E_h/\text{Bohr}}{e})$	7.280909 (forward reaction) 11.736088 (backward reaction)	11.822059 (forward reaction) 6.927205 (backward reaction)
<u>Barrier-recrossing</u> κ_{LZ}	0.77856930	0.63139145
C (kcal/mol)	0.350651	0.253203
$\lvert\bar{v}_E\rvert$ $(\frac{E_h/\text{Bohr}}{e}\ fs^{-1})$	0.000406	0.000413
$\lvert S_2\text{-}S_1\rvert$ (kcal mol^{-1}/ $\frac{E_h/\text{Bohr}}{e}$)	123.609228	103.900885
<u>Timescale:</u> τ (ps)	2.780294	5.321732

References

1. S. Roy, M. Brehm, S. Sharma, F. Wu, D. Maltsev, P. Halstenberg, L. Gallington, S. Mahurin, S. Dai, A. Ivanov, C. Margulis and V. Bryantsev, Unraveling Local Structure of Molten Salts via X-Ray Scattering, Raman Spectroscopy, and Ab Initio Molecular Dynamics, *J. Phys. Chem. B.*, 2021, **125**, 5971–5982.
2. R. Marcus, Chemical + Electrochemical Electron-Transfer Theory, *Annual Review of Physical Chemistry*, 1964, **15**, 155-&.
3. M. Newton and N. Sutin, Electron-Transfer Reactions in Condensed Phases, *Annual Review of Physical Chemistry*, 1984, **35**, 437-480.
4. S. Roy, S. Sharma, W. V. Karunaratne, F. Wu, R. Gakhar, D. S. Maltsev, P. Halstenberg, M. Abeykoon, S. K. Gill, Y. Zhang, M. M. Shannon, S. Dai, V. S. Bryantsev, C. J. Margulis and A. S. Ivanova, X-ray scattering reveals ion clustering of dilute chromium species in molten chloride medium, *Chem. Sci.*, 2021, DOI: 10.1039/D1SC01224J.
5. S. Roy, G. Schenter, J. Napoli, M. Baer, T. Markland and C. Mundy, Resolving Heterogeneous Dynamics of Excess Protons in Aqueous Solution with Rate Theory, *Journal of Physical Chemistry B*, 2020, **124**, 5665-5675.
6. L. D. Landau, Theory of Energy Transfer on Collisions., *Phys. Z.Sowjet.*, 1932, **1**, 88.
7. C. Zener, Non-adiabatic Crossing of Energy-Levels, *Current Contents/physical Chemical & Earth Sciences*, 1983, 24-24.
8. M. Salanne, L. Siqueira, A. Seitsonen, P. Madden and B. Kirchner, From molten salts to room temperature ionic liquids: Simulation studies on chloroaluminate systems, *Faraday Discussions*, 2012, **154**, 171-188.
9. S. Nose, A unified formulation of the constant temperature molecular-dynamics methods, *Journal of Chemical Physics*, 1984, **81**, 511-519.

10. W. Hoover, Canonical dynamics - equilibrium phase-space distributions, *Physical Review a*, 1985, **31**, 1695-1697.
11. A. Aguado and P. Madden, Ewald summation of electrostatic multipole interactions up to the quadrupolar level, *Journal of Chemical Physics*, 2003, **119**, 7471-7483.
12. T. D. Kühne, M. Iannuzzi, M. Del Ben, V. V. Rybkin, P. Seewald, F. Stein, T. Laino, R. Z. Khaliullin, O. Schütt and F. Schiffmann, CP2K: An electronic structure and molecular dynamics software package-Quickstep: Efficient and accurate electronic structure calculations, *The Journal of Chemical Physics*, 2020, **152**, 194103.
13. J. VandeVondele, M. Krack, F. Mohamed, M. Parrinello, T. Chassaing and J. Hutter, QUICKSTEP: Fast and accurate density functional calculations using a mixed Gaussian and plane waves approach, *Computer Physics Communications*, 2005, **167**, 103-128.
14. Y. Zhang and W. Yang, Comment on "Generalized gradient approximation made simple", *Physical Review Letters*, 1998, **80**, 890-890.
15. J. Perdew, K. Burke and M. Ernzerhof, Comment on "Generalized gradient approximation made simple" - Reply, *Physical Review Letters*, 1998, **80**, 891-891.
16. J. Perdew, K. Burke and M. Ernzerhof, Generalized gradient approximation made simple, *Physical Review Letters*, 1996, **77**, 3865-3868.
17. S. Grimme, J. Antony, S. Ehrlich and H. Krieg, A consistent and accurate ab initio parametrization of density functional dispersion correction (DFT-D) for the 94 elements H-Pu, *Journal of Chemical Physics*, 2010, **132**.
18. J. VandeVondele and J. Hutter, Gaussian basis sets for accurate calculations on molecular systems in gas and condensed phases, *Journal of Chemical Physics*, 2007, **127**.
19. S. Goedecker, M. Teter and J. Hutter, Separable dual-space Gaussian pseudopotentials, *Physical Review B*, 1996, **54**, 1703-1710.
20. S. Roy, M. Brehm, S. Sharma, F. Wu, D. S. Maltsev, P. Halstenberg, L. C. Gallington, S. M. Mahurin, S. Dai, A. S. Ivanov, C. J. Margulis and V. S. Bryantsev, Unraveling Local Structure of Molten Salts via X-ray Scattering, Raman Spectroscopy, and Ab Initio Molecular Dynamics, *The Journal of Physical Chemistry B*, 2021, **125**, 5971-5982.
21. G. Martyna, M. Klein and M. Tuckerman, Nose-hoover chains - the canonical ensemble via continuous dynamics, *Journal of Chemical Physics*, 1992, **97**, 2635-2643.
22. M. Brehm, M. Thomas, S. Gehrke and B. Kirchner, TRAVIS—A free analyzer for trajectories from molecular simulation, *The Journal of chemical physics*, 2020, **152**, 164105.
23. R. D. King-Smith and D. Vanderbilt, Theory of polarization of crystalline solids, *Physical Review B*, 1993, **47**, 1651.
24. R. Resta, Macroscopic electric polarization as a geometric quantum phase, *Europhysics Letters*, 1993, **22**, 133.
25. J. Hutter, M. Iannuzzi, F. Schiffmann and J. VandeVondele, cp2k: atomistic simulations of condensed matter systems, *Wiley Interdisciplinary Reviews: Computational Molecular Science*, 2014, **4**, 15-25.
26. M. J. Frisch, G. W. Trucks, H. B. Schlegel, G. E. Scuseria, M. A. Robb, J. R. Cheeseman, G. Scalmani, V. Barone, G. A. Petersson, H. Nakatsuji, X. Li, M. Caricato, A. V. Marenich, J. Bloino, B. G. Janesko, R. Gomperts, B. Mennucci, H. P. Hratchian, J. V. Ortiz, A. F. Izmaylov, J. L. Sonnenberg, D. Williams-Young, F. Ding, F. Lipparini, F. Egidi, J. Goings, B. Peng, A. Petrone, T. Henderson, D. Ranasinghe, V. G. Zakrzewski, J. Gao, N. Rega, G. Zheng, W.

Liang, M. Hada, M. Ehara, K. Toyota, R. Fukuda, J. Hasegawa, M. Ishida, T. Nakajima, Y. Honda, O. Kitao, H. Nakai, T. Vreven, K. Throssell, J. A. Montgomery, Jr., J. E. Peralta, F. Ogliaro, M. J. Bearpark, J. J. Heyd, E. N. Brothers, K. N. Kudin, V. N. Staroverov, T. A. Keith, R. Kobayashi, J. Normand, K. Raghavachari, A. P. Rendell, J. C. Burant, S. S. Iyengar, J. Tomasi, M. Cossi, J. M. Millam, M. Klene, C. Adamo, R. Cammi, J. W. Ochterski, R. L. Martin, K. Morokuma, O. Farkas, J. B. Foresman and D. J. Fox, Gaussian 16, Revision A.03.*Journal*, 2016.

27. C. Bernardes, AGGREGATES: Finding Structures in Simulation Results of Solutions, *Journal of Computational Chemistry*, 2017, **38**, 753-765.
28. L. Wang, R. McGibbon, V. Pande and T. Martinez, Automated Discovery and Refinement of Reactive Molecular Dynamics Pathways, *Journal of Chemical Theory and Computation*, 2016, **12**, 638-649.